



OPEN

Multi-omics reveals the role of ENO1 in bladder cancer and constructs an epithelial-related prognostic model to predict prognosis and efficacy

Zhixiong Su^{1,2}, Lijie You^{1,2}, Yufang He^{1,2}, Jingbo Chen^{1✉}, Guifeng Zhang^{1✉} & Zhenhua Liu^{1✉}

α -Enolase (*ENO1*) is a crucial molecular target for tumor therapy and has emerged as a research hotspot in recent decades. Here, we aimed to explore the role of *ENO1* in bladder cancer (BLCA) and then construct a signature to predict the prognosis and treatment response of BLCA. Firstly, we found *ENO1* was highly expressed in BLCA tissues, as verified by IHC, and was associated with poor prognosis. The analysis of the tumor immune microenvironment by bulk RNA-seq and scRNA-seq showed that *ENO1* was associated with CD8+ T-cell exhaustion. Additionally, the results in vitro showed that *ENO1* could promote the proliferation and invasion of BLCA cells. Then, the analysis of epithelial cells (ECs) revealed that *ENO1* might promote BLCA progression by metabolism, the cell cycle and some carcinogenic pathways. A total of 249 hub genes were obtained from differentially expressed genes between *ENO1*-related ECs, and we used LASSO analysis to construct a novel signature that not only accurately predicted the prognosis of BLCA patients but also predicted the response to treatment for BLCA. Finally, we constructed a nomogram to better guide clinical application. In conclusion, through multi-omics analysis, we found that *ENO1* was overexpressed in bladder cancer and associated with poor prognosis, CD8+ T-cell exhaustion and epithelial heterogeneity. Moreover, the prognosis and treatment of patients can be well predicted by constructing an epithelial-related prognostic signature.

Bladder cancer (BLCA) is one of the most common malignant tumors in the genitourinary system, with approximately 430,000 cases per year worldwide^{1,2}. Its incidence is four times higher in men than in women, and it ranks as the sixth most frequently diagnosed malignancy among men³. Contributing to the progress in early detection, the majority of cases are resectable at diagnosis, with a 5-year survival rate of up to 77.1%, whereas approximately 50–70% of those will suffer recurrence within 5 years⁴. In addition, 10–15% of patients encounter metastasis at the time of diagnosis, with a 5-year survival rate as low as 4.75². Tumor heterogeneity, regardless of whether it is at either the molecular or cellular level, results in this apparent divergence⁵. Therefore, it is imperative to search for new therapeutic targets or biomarkers in the management of BLCA.

α -enolase (*ENO1*), also known as 2-phospho-D-glycerate hydrolase, is a glycolytic enzyme that catalyzes the conversion of 2-phosphoglycerate to phosphoenolpyruvate during glycolysis⁶. Studies have confirmed that *ENO1* is overexpressed in more than 70% of cancers and is also associated with poor patient outcomes^{7–9}. It can promote cancer progression by sustaining proliferative signaling^{10,11}, activating invasion and metastasis^{10,12,13}, inducing angiogenesis¹⁴, deregulating cellular energy¹⁵ and avoiding immune destruction^{16,17}. Additionally, *ENO1* was reported to reduce tumor cell tolerance to hypoxia via the aerobic glycolysis pathway and resulted in tumor angiogenesis^{18,19}. However, previous studies have mostly focused on cell lines, making it difficult to reveal the true tumor microenvironment. With the development of technology, single-cell RNA sequencing (scRNA-seq) is used to define the global gene expression profile of a single cell, which allows us to explore the hidden heterogeneity in a cell population²⁰. Hence, we sought to reveal the role of *ENO1* in BLCA through scRNA-seq and bulk RNA-seq data.

¹Department of Oncology, Shengli Clinical Medical College of Fujian Medical University, Fujian Provincial Hospital, No. 134, East Street, Fuzhou 350001, Fujian, People's Republic of China. ²These authors contributed equally: Zhixiong Su, Lijie You and Yufang He. ✉email: 13635294192@163.com; 984386537@qq.com; liuzhenhua6909@163.com

In the present study, we showed that *ENO1* was overexpressed in BLCA tissues and was correlated with poor prognosis in BLCA patients. Then, we found that *ENO1* may be associated with CD8+ T-cell exhaustion and that there was heterogeneity in epithelial cells (ECs) with different *ENO1* expression levels. Next, we screened the hub genes by differential expression analysis and constructed a novel signature to predict the prognosis and response to treatments in BLCA patients. Finally, we developed a nomogram combining the novel signature and clinicopathological features to facilitate its clinical application in the prognosis of BLCA.

Materials and methods

Patients and datasets

The Cancer Genome Atlas (TCGA, <https://portal.gdc.cancer.gov/>) bladder cancer RNA-seq profiling in the form of fragments per kilobase million (FPKM) and corresponding clinicopathological data were collected from the TCGA database. The RNA-seq data and clinicopathological data of GSE13507 were obtained from the Gene Expression Omnibus (GEO) database. We removed patients with a survival time of 0. Finally, 403 patients in TCGA-BLCA and 165 patients in GSE13507 were used in this study. The RNA-seq profiles and clinical data of the “IMvigor 210” cohort were derived from <http://research-pub.gene.com/IMvigor210CoreBiologies/>²¹. Furthermore, 10 pairs of frozen, surgically resected tumor specimens were acquired from patients pathologically diagnosed with BLCA at the Fujian Provincial Hospital (FPH) between December 2015 and December 2017. This study was approved by the ethics committee of the FPH. The clinical and pathological characteristics of the above patients are shown in Supplementary Table 1.

scRNA-seq data quality control and processing

We downloaded the scRNA-seq data of CD8+ T cells in GSE149652, which included 10,763 CD8+ T cells, to explore the relationship between *ENO1* and CD8+ T cells²². The scRNA-seq profiling of 7 primary BLCA cases with no treatment was obtained from GSE135337 to analyze the heterogeneity of malignant epithelial cells (ECs)²³. Using the “Seurat” package²⁴, we excluded cells with less than 200 genes detected and more than 10% mitochondrial gene proportion. Based on the top 1500 variable genes across all cell samples, PCA and t-SNE were then performed to classify the cell samples, and the marker genes were screened with $|\log_2FC| > 0.5$ and adjusted $P < 0.05$ filtering²⁵. The results of quality control in GSE149652 and GSE135337 are shown in supplementary Fig. 1 and supplementary Fig. 2, respectively. Finally, we obtained 10,483 cells in GSE149652 and 36,695 cells in GSE135337.

Then, we annotated the cell categories in GSE149652 based on the marker genes with CellMarker (<http://biocc.hrbmu.edu.cn/CellMarker/>)²⁶ and annotated the cell categories in GSE135337 by using the R package “singleR”²⁷. In GSE135337, we further screened 35,945 ECs after using “singleR” annotation for follow-up analysis. The R package “Monocle2” was used to perform trajectory analysis²⁸. The R package “scMetabolism” was used to calculate the activity score of metabolic pathways²⁹. In addition, the intersection of differential genes between different ECs were taken as hub genes.

Differential expression and prognosis analysis of *ENO1*

Using the “limma” and “survminer” R packages, we analyzed the differential expression between normal and tumor tissues and the prognostic value of *ENO1*. Furthermore, we used immunohistochemistry (IHC) to verify the difference in *ENO1* protein expression between tumor and normal tissues. IHC staining of paraffin-embedded tissues with an antibody against *ENO1* (1:200, 11, 204-1-AP, Proteintech) was performed according to the standard procedures as previously described and was evaluated by two independent pathologists. As described previously, the percentage (P) and intensity (I) of cytoplasmic or membrane expression were multiplied to generate the H score ($H \text{ score} = P \times I$)³⁰.

Cell culture and transfection

The human BLCA cell line HT1376 was cultured in RPMI-1640 medium (Invitrogen) at 37 °C with 5% CO₂. All media were supplemented with 10% FBS. For the knockdown assay, small interfering RNAs targeting *ENO1* (si-*ENO1*-296, si-*ENO1*-664, si-*ENO1*-791 and si-*ENO1*-880) were applied, and scramble siRNAs (siNC) were used as the negative control. The siRNA sequences targeting *ENO1* can be found in Supplementary Table 2.

Western blot assays

Antibodies against *ENO1* (1:1000, XC1033) were purchased from BIOTECH. Briefly, cells were lysed by RIPA buffer with protease and phosphatase inhibitor cocktail following the manufacturer’s specification, and then the concentrations were measured and normalized by BCA assay. Western blotting was performed according to the standard methods as depicted in the manufacturer’s specification and previous studies³¹.

Quantitative real-time PCR

Total RNA was isolated from the cultured cells using TRIzol reagent (TaKaRa). RNA was then converted into cDNA by applying the TaKaRa PrimeScript™ RT Master Mix (Perfect Real Time) Kit. A ChamQ Universal SYBR qPCR Master Mix Kit from Norvezan was used to examine gene mRNA expression levels using a PCR instrument (Thermo Fisher). The specific primer sequences are listed in Supplementary Table 2.

Cell counting kit-8 assay

Cells were plated in 96-well plates at 1×10^4 per well, and 10 μ l of CCK-8 solution (A311, Vazyme) was added to each well after 24 and 48 h. Then, the cells were incubated for 1 h at 37 °C and 5% CO₂. Finally, the optical absorbance was measured at 450 nm. Each experiment was performed in triplicate.

Wound healing assay

Cells from each group were plated into 6-well plates at approximately 95% confluence. Then, we used a 200 μ l pipette tip to make symmetrical wounds. After being washed twice with PBS, the cells were incubated with serum-free RPMI-1640 medium for 24 h (or 48 h). Migration pictures were taken at 0 h and 24 h (or 48 h) after drawing the wound. The wound distance of each group at 40 \times magnification was measured by ImageJ software. Each experiment was performed in triplicate.

TME and immunotherapy benefits analysis

The “ESTIMATE” R package was utilized to calculate the immune scores, stromal scores, and ESTIMATE scores, which can be used to evaluate the abundance of immune cells and stromal cells in the tumor microenvironment (TME). The infiltration and function of immune cells were quantified by single-sample gene set enrichment analysis (ssGSEA) via the “gsva” R package³². Correlation analysis between the CD8+ T-cell infiltration level and *ENO1* expression or prognosis in bladder cancer patients was obtained from the Tumor Immune Estimation Resource (TIMER, <https://cistrome.shinyapps.io/timer/>) website³³. Immune activity scores of anticancer immunity across the seven-step cancer-immunity cycle for BLCA patients were downloaded from the website Tracking Tumor Immunophenotype (TIP, <http://biocc.hrbmu.edu.cn/TIP/index.jsp>)³⁴. Immunophenoscore (IPS) scores were obtained from the Cancer Immuneome Database (TCIA, <https://tcia.at/home>), which can predict patient response to immunotherapy³⁵.

Functional analysis

Gene set enrichment analysis (GSEA), Gene Ontology biological processes (GO-BP) and Kyoto Encyclopedia of Genes and Genomes (KEGG) analysis^{36–38} were used to analyze the main functions using the R package “clusterProfiler”³⁹.

Consensus clustering analysis

We explored the prognostic value of hub genes by clustering TCGA-BLCA patients into different clusters using the “ConsensusClusterPlus” R package⁴⁰. The cumulative distribution function (CDF) and delta area were considered to determine the optimal number of groups (k). A relatively high consistency, a low variation coefficient and a significant increase in the CDF curve area were used to determine the cluster number. Then, we used GSE13507 to verify the results of the consensus clustering analysis.

Construction and validation of a prognostic signature in BLCA

We screened the prognostically significant hub genes ($P < 0.05$) by univariate Cox regression analysis. Least absolute shrinkage and selection operator (LASSO) regression is known to be able to remove unimportant variables via the regression coefficients penalizing the size of the parameters. Applying the LASSO regression method, feature selection and predictive signature building was done⁴¹. Therefore, we constructed a novel signature via LASSO analysis to predict the overall survival (OS) of BLCA patients in the TCGA cohort using the R package “glmnet”⁴². The risk score for each patient was determined using the following formula:

$$\text{Risk score} = \sum_{i=0}^n \text{Coef}(i) \times x(i)$$

Thereafter, the patients were classified into low- and high-risk groups based on the median risk score. We determined the prognostic ability of the novel signature by generating Kaplan–Meier survival curves and receiver operating characteristic (ROC) curves using the R packages “survminer” and “survivalROC”. The GSE13507 cohort was used to verify the prognostic performance of the novel signature in the same manner as mentioned above.

Drug sensitivity analysis

The sensitivity of BLCA patients to each commonly used drug was calculated by IC50 values using the “pRRophetic” package, and the corresponding data were obtained from the GDSC database⁴³.

Construction of the nomogram

Univariate and multivariate Cox regression were used to screen the independent prognostic factors for BLCA patients in TCGA, based on which we constructed a nomogram using the “rms” package. Additionally, we evaluated this nomogram using calibration curves, ROC curves, and decision-making curves (DCAs).

Statistical analysis

The normality of the variables was tested by the Shapiro–Wilk test. Differences between two normally distributed groups were determined by Student’s t test, and the Wilcoxon test measured differences between two non-normally distributed variables. One-way analysis of variance (ANOVA) tests were used as a parametric method for multiple group comparisons, while Kruskal–Wallis tests were used as a nonparametric method. Based on

correlation coefficients, Pearson correlation and distance correlation analyses were performed. Chi-square contingency tests were used for contingency table analyses. The Benjamini–Hochberg method was applied for P values to FDR conversion in the DEG analysis. All tests were two-sided, and $P < 0.05$ was considered statistically significant. All statistical analyses were performed using RStudio version 4.1.0, and a two-sided $P < 0.05$ was deemed statistically significant.

Result

ENO1 was overexpressed in BLCA and associated with poor prognosis

Figure 1 illustrates the research process of this study. By differential analysis, we observed higher expression of *ENO1* in BLCA tissues than in normal tissues, both in paired and unpaired samples (all $P < 0.05$; Fig. 2A–C). Based on the median expression of *ENO1*, we classified BLCA patients into low- and high-expression groups. As shown in Fig. 2D–F, the high-expression group was positively correlated with worse OS and disease-specific survival (DSS) in BLCA patients (all $P < 0.05$). Moreover, to verify the differential expression of *ENO1* protein, we conducted IHC on tumor and adjacent tumor samples of FPH, and the results showed a higher H score for *ENO1* in tumor tissues than in normal tissues ($P < 0.05$; Fig. 2G). Figure 2H displayed typical results of IHC staining. Collectively, these results suggested that *ENO1* played an essential role in the prognosis of BLCA.

ENO1 was relevant to CD8+ T-cell exhaustion

To investigate the influence of *ENO1* on the TME, we explored the correlation between *ENO1* expression and immune cell infiltration. By ssGSEA, we found that most of the 16 infiltrating immune cells, including CD8+ T cells and Tregs, had a higher abundance of infiltrating immune cells in the high-expression group (all $P < 0.05$; Fig. 3A). To explore the underlying mechanism, we performed the corresponding immune function analysis, and the results revealed that heightened levels of the CD8 TCR pathway were elevated in the high-expression group, as well as the immunosuppressive pathways of T-cell coinhibition and APC coinhibition (all $P < 0.05$; Fig. 3A). Furthermore, analysis of immune activity scores across the seven steps of the cancer-immunity cycle showed that the activity score of step 1 and several steps of step 4 was high in the high-expression group (Fig. 3B). However, the antitumor effect phase (steps 5–7) of immune cells was not significantly different (Fig. 3B). In addition, we found that samples in the high-expression groups had significantly higher immune scores and ESTIMATE scores than those in the low-expression group (all $P < 0.05$; Fig. 3C). These findings suggested that the activity of antitumor immune cells may be suppressed in high-expression group patients.

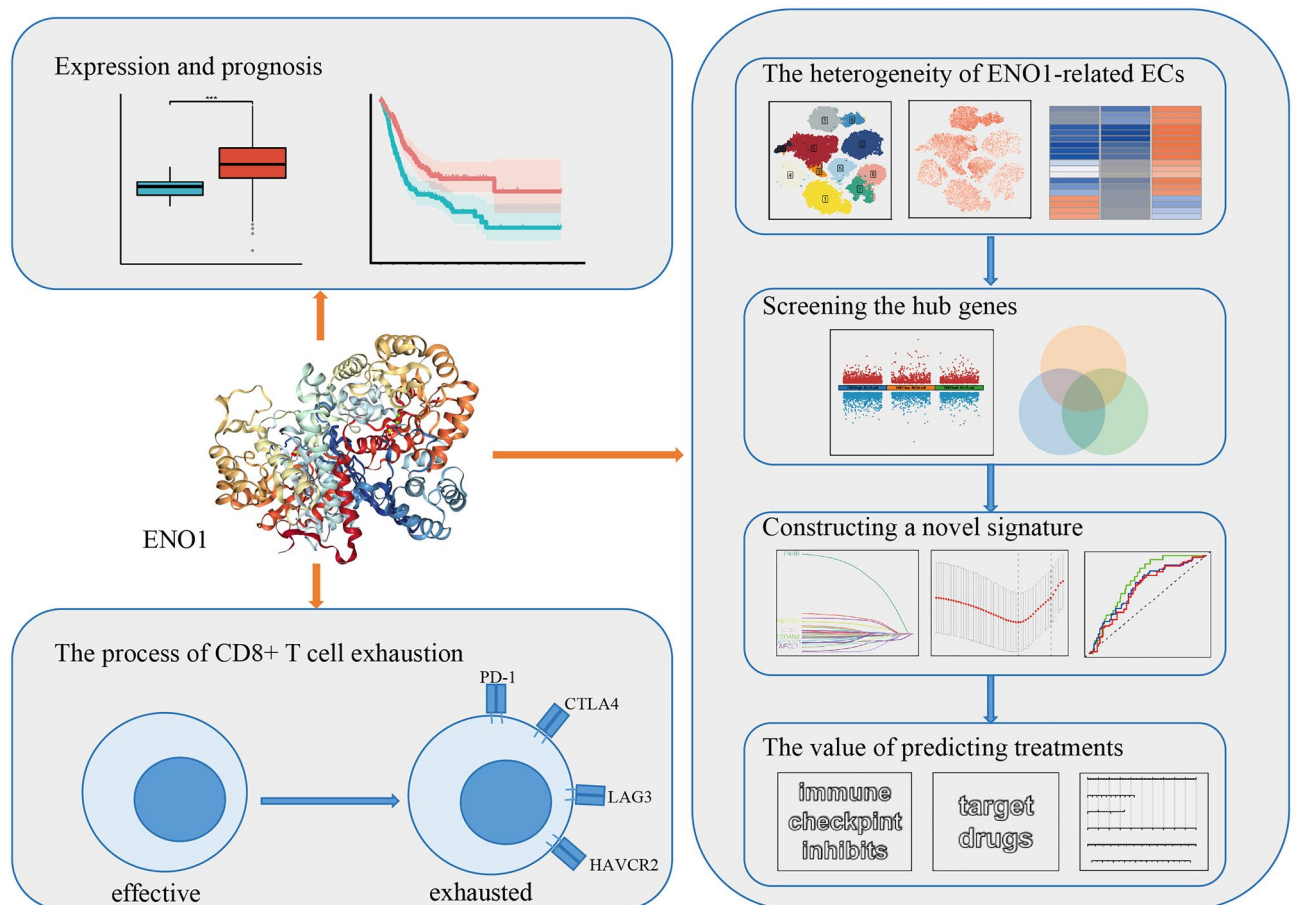


Figure 1. Flow chart of this study.

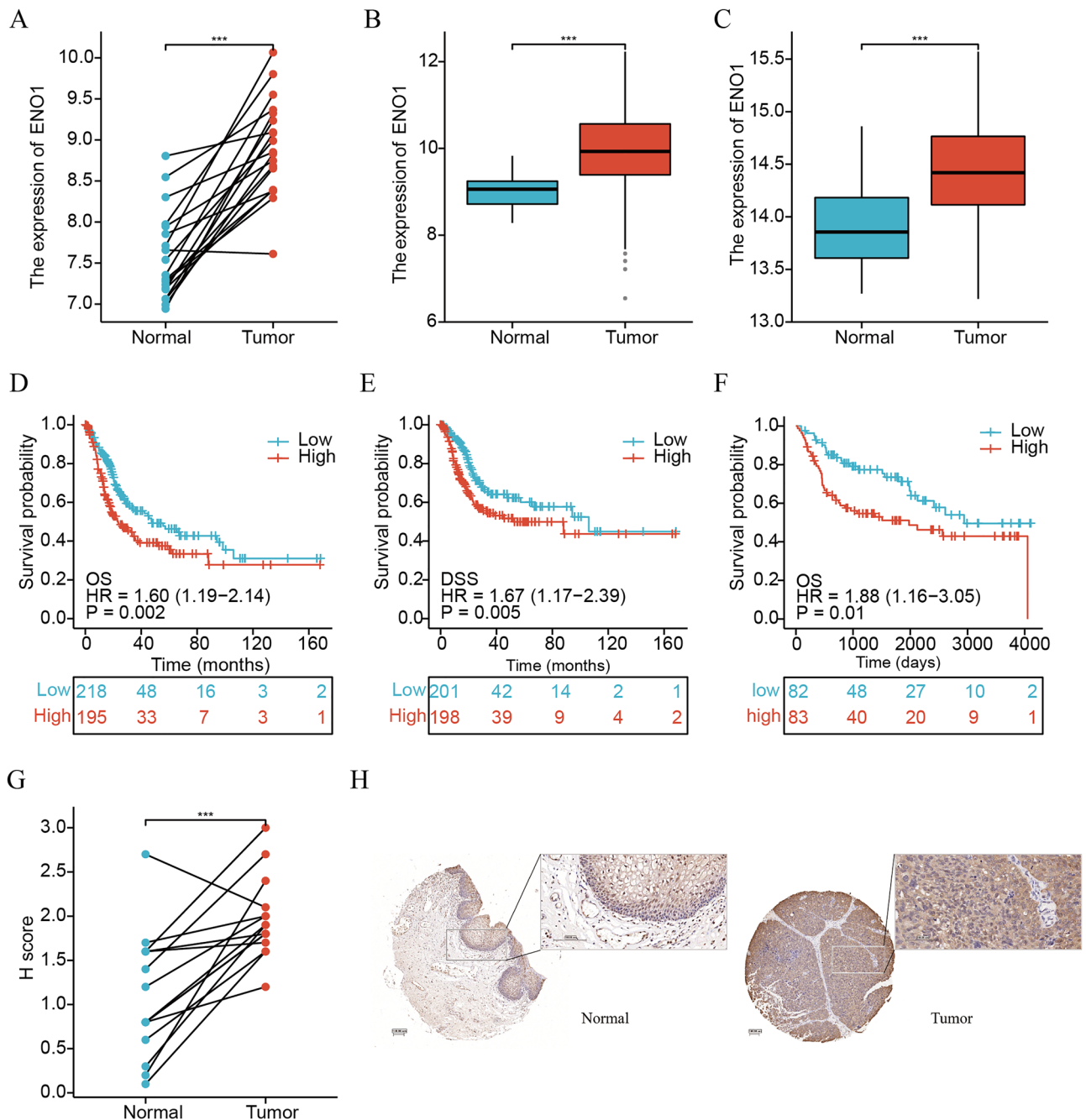


Figure 2. *ENO1* was overexpressed in BLCA tissues and associated with poor prognosis. Differential expression among paired samples (A) and unpaired samples (B) in the TCGA cohort. (C) Differential expression among unpaired samples in the GSE13507 cohort. Kaplan–Meier survival curve of OS (D) and DSS (E) between the high- and low-expression groups of *ENO1* in the TCGA cohort. (F) Kaplan–Meier survival curve of OS between the high- and low-expression groups of *ENO1* in the GSE13507 cohort. (G) Differential H score among paired samples by IHC in the PFH cohort. (H) Typical staining histochemical results of normal and tumor tissues in the PFH cohort. *** $P < 0.001$; ** $0.001 < P < 0.01$; * $0.01 < P < 0.05$; ns: $P > 0.05$.

To further explore the mechanism, we found that CD8+ T cells were positively correlated with *ENO1* expression ($R = 0.332$, $P < 0.001$; Fig. 3D) and associated with poor prognosis ($P < 0.05$; Fig. 3E) in BLCA using TIMER website analysis. T-cell exhaustion (TEX) is characterized by poor effector functions and increased expression of inhibitory receptors such as *CD274*, *CD276*, *PDCD1*, *CTLA4*, *TIGIT*, *HAVCR2* and *LAG3*⁴⁴. Therefore, we explored the relationship between *ENO1* and inhibitory receptors, which suggested that *ENO1* was positively correlated with the expression of inhibitory receptors (all $P < 0.05$; Fig. 3F). Furthermore, we obtained IHC images of *ENO1* protein with different *PD-1* expression levels and found that patients with high *PD-1* expression had higher *ENO1* expression (Fig. 3G, H). Consequently, we hypothesized that the highly infiltrated CD8+ T cells in the high-expression group may have been exhausted.

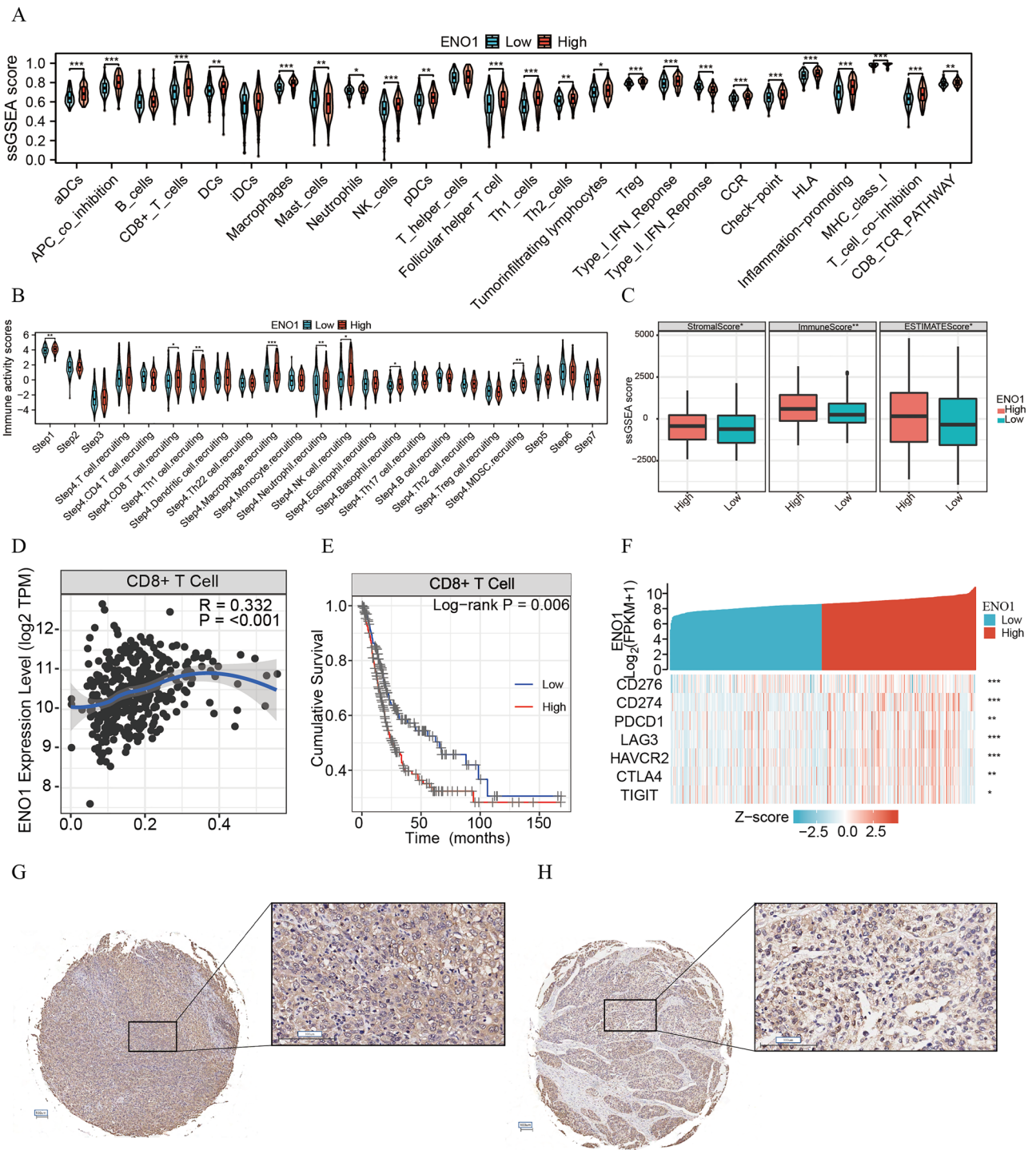


Figure 3. *ENO1* was correlated with a suppressive antitumor microenvironment and exhausted CD8+ T cells. (A) The infiltration levels of 16 immune cells and the activation levels of immune-related pathways of the high- and low-expression groups by ssGSEA. (B) Differences in cancer immune cycling activity between the high- and low-expression groups. (C) Differences in ESTIMATE score, immune score and stromal score among the high- and low-expression groups. (D) Scatter plot of the association between *ENO1* and CD8+ T cells. (E) Kaplan–Meier survival curve of OS between the high- and low-infiltrating level groups of CD8+ T cells. (F) Heatmap showing the relationship between *ENO1* and T-cell exhaustion markers. Typical staining histochemical results of *PD-1* expression greater than 50% (G) and *PD-1* expression less than 1% (H) in the PFH cohort. *** $P < 0.001$; ** $0.001 < P < 0.01$; * $0.01 < P < 0.05$; ns: $P > 0.05$.

Given that CD8+ T cells may have been exhausted in the *ENO1* high-expression group, we tried to explore the association between *ENO1* and exhausted CD8+ T cells in the BLCA scRNA-seq dataset. The t-SNE map showed that CD8+ T cells were divided into 9 different clusters (Fig. 4A). By annotating the marker genes of different t-SNE clusters, we found that clusters 0, 2, 3, 6, 7 and 8 were “exhausted CD8+ T cells” (including 6564 cells), clusters 1 and 5 were “effector CD8+ T cells” (including 2752 cells), and cluster 4 was “memory CD8+ T cells” (including 1167 cells) (Supplementary Fig. 1E, F). Then, we analyzed the expression of immunosuppressive receptors (*CD274*, *PDCD1*, *CTLA4*, *TIGIT*, *LAG3* and *HAVCR2*) between different clusters and found that these genes were more highly expressed in exhausted CD8+ T cells than in effector CD8+ T cells and memory CD8+ T cells (Fig. 4B). We next established a pseudotemporal trajectory to trace cell differentiation. The CD8+ T-cell trajectory was reconstructed using Monocle2, which revealed that the pseudotime increased from effector CD8+ T cells and memory CD8+ T cells to exhausted CD8+ T cells (Fig. 4C, D). Moreover, we explored the trend of *ENO1* and immunosuppressive gene expression over pseudotime and found that their expression increased gradually (Fig. 4E). Hence, we believed that the increase in *ENO1* was associated with the process of CD8+ T-cell exhaustion.

***ENO1* knockdown inhibits cell proliferation and invasion in BLCA**

To explore the role of *ENO1* in BLCA cells, we performed CCK-8 and wound healing assays in HT1376 cell lines in vitro. First, we transfected different siRNAs into HT1376 cell lines and verified *ENO1* knockdown by western blotting (Fig. 5A) and qRT-PCR ($P < 0.05$; Fig. 5B). Next, we selected siENO1-664 for further analysis. The CCK-8 assay showed that knockdown of *ENO1* significantly inhibited the proliferation of HT1376 cells ($P < 0.05$; Fig. 5C). In addition, the wound healing results suggested that *ENO1* knockdown inhibited the invasion ability of cells ($P < 0.05$; Fig. 5D, E). In conclusion, these in vitro results confirmed that the proliferation and invasion abilities of BLCA cells were correspondingly impaired after *ENO1* expression was decreased.

***ENO1*-related EC subgroups have heterogeneity**

Considering that *ENO1* was highly expressed in tumor cells and positively correlated with malignant phenotypes, we performed further analysis of epithelial cells (ECs) in the scRNA-seq data. First, we annotated 35945 ECs from GSE135337 (Supplementary Fig. 2). Then, we reclassified ECs into 11 clusters through t-SNE analysis and found that clusters 0, 3, 5, 8, and 9 had high *ENO1* expression, clusters 1, 4, and 10 had moderate *ENO1* expression, and clusters 2, 6, and 7 had low *ENO1* expression (Fig. 6A). The t-SNE map showed the expression of *ENO1* in every ECs (Fig. 6B). Based on the expression of *ENO1*, we annotated ECs as *ENO1*^{high}-BLCA cells, *ENO1*^{mid}-BLCA cells and *ENO1*^{low}-BLCA cells (Fig. 6C), and Fig. 6D shows the differential expression of *ENO1* between them (all $P < 0.05$). To explore potential heterogeneity between different ECs, we performed GSVA. The results showed that *ENO1*^{high}-BLCA cells had higher energy metabolism pathway activity (including glycolysis, fatty acid metabolism, bile acid metabolism and heme metabolism), higher cell cycle-related pathway activity (including the G2M checkpoint and E2F targets) and higher epithelial-mesenchymal transition (EMT) and PI3K/AKT/mTOR pathway activity (Fig. 6E). In addition, through metabolic activity analysis, we found that *ENO1* expression was positively correlated with the activities of fatty acid degradation, glycolysis and pyruvate metabolism pathways (all $P < 0.05$, Fig. 6F). These results suggested that there was heterogeneity among ECs with different *ENO1* expression levels and that *ENO1* may contribute to poor prognosis by enhancing EC energy metabolism, regulating the cell cycle, and promoting EMT.

Obtaining the hub genes between different ECs

The Manhattan map showed that genes were upregulated and downregulated between different ECs (Fig. 7A). By taking the intersection, we obtained 249 hub genes (Fig. 7B). GO-BP analysis showed that hub genes were mainly concentrated in energy metabolism and apoptosis regulation (Fig. 7C), and KEGG analysis showed that hub genes were involved in energy metabolism, ribosome function and carcinogenic pathways (Fig. 7D). To probe the effect of prognosis from hub genes, we performed consensus clustering analysis in the TCGA cohort. We observed a relative change in the CDF of the consensus cluster from $k = 2$ to $k = 9$ (Supplementary Fig. 3A); the delta area under the CDF curve from $k = 2$ to 9 is depicted in Supplementary Fig. 3A. The corresponding heatmap presents the results of this consensus from $k = 2$ to 9 ($k = 2$, Fig. 7E; $k = 1$, $k = 3-9$, Supplementary Fig. 3A). The optimal cluster number was thus determined to be $k = 2$ after comprehensive consideration. Then, a significant difference in OS was observed between patients C01 and C02 ($P = 0.019$; Fig. 7F). In addition, we conducted the above analysis on GSE13507 and found that the results were consistent with those of the TCGA cohort (Fig. 7G, H, Supplementary Fig. 3B).

Construction and validation of the novel prognostic signature

The TCGA cohort was used as the training cohort to evaluate the prognostic value of the above 249 hub genes (Supplementary Table 3), among which 29 hub genes were identified as prognostic genes (all $P < 0.05$; Supplementary Table 4). Next, among the 29 hub genes, six (*AKR1B1*, *APOL1*, *TSPAN8*, *SPOCD1*, *P4HB* and *CTSE*) were screened as candidate genes to construct the prognostic prediction signature using LASSO regression analysis (Fig. 8A–C). The risk score of the novel signature was calculated according to the following formula: Risk score = [*AKR1B1* expression*(0.000487466)] + [*APOL1* expression*(- 0.254539811)] + [*TSPAN8* expression*(- 0.050694694)] + [*SPOCD1* expression*(- 0.028378046)] + [*P4HB* expression*(0.445721382)] + [*CTSE* expression*(- 0.067550766)].

Taking the median risk score as the cutoff value, patients in the TCGA set were divided into two subgroups: low- and high-risk. The K–M survival curve showed that the median OS was significantly shorter in the high-risk subgroup than in the low-risk subgroup ($P < 0.001$; Fig. 8D). ROC analysis revealed that the novel

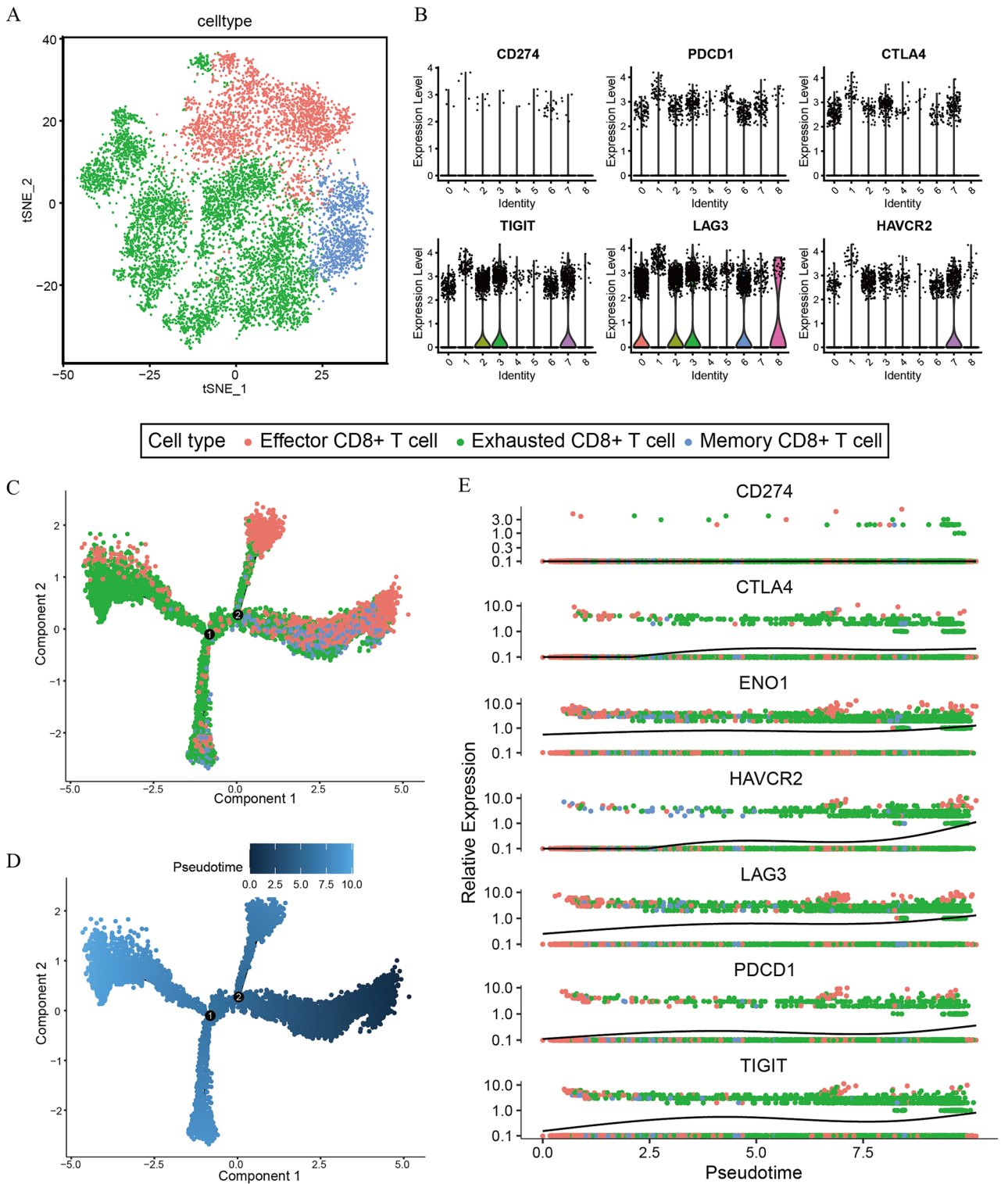


Figure 4. *ENO1* was associated with exhausted CD8+ T cells in BLCA by single-cell analysis. (A) Annotations for CD8+ T-cell subtypes. (B) Differential expression of immunosuppressive receptors between clusters 0–9. (C, D) The results of pseudotime analysis in different CD8+ T-cell subtypes. (E) The expression of *ENO1* and immunosuppressive receptors increased with pseudotime.

signature exhibited an excellent predictive capability in the TCGA set (AUC values at 1 year, 3 years and 5 years: 0.686, 0.654, and 0.656, respectively; Fig. 8E). Figure 8F shows the changes in patient survival status and the

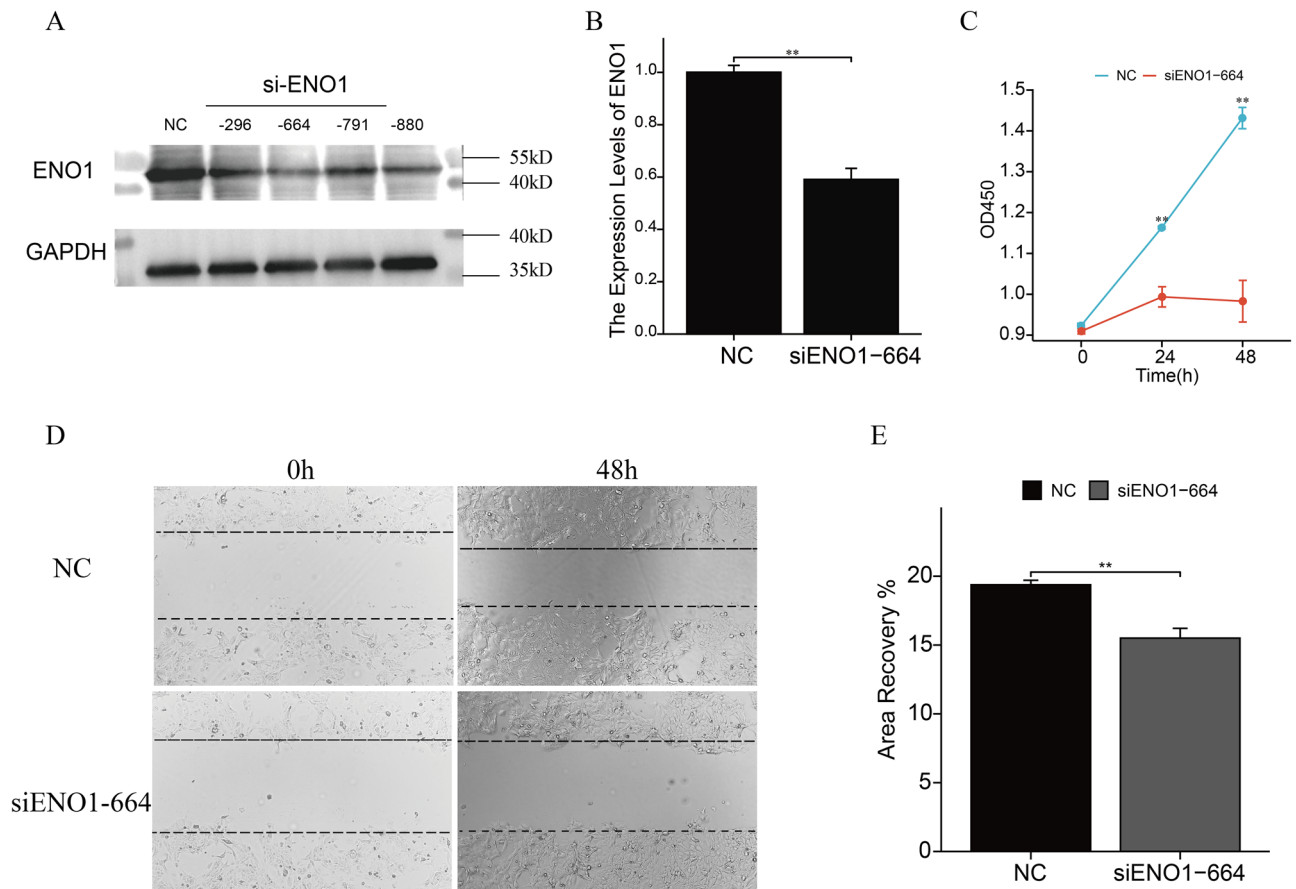


Figure 5. *ENO1* knockdown inhibits cell proliferation and invasion. (**A, B**) shENO1-664 significantly inhibited the expression of *ENO1* in HT1376 cells (original blots are presented in Supplementary Fig. 5). (**C**) The results of CCK-8 assays. (**D, E**) The results of wound healing assays. *** $P < 0.001$; ** $0.001 < P < 0.01$; * $0.01 < P < 0.05$; ns: $P > 0.05$.

expression of signature genes with the change in risk score, indicating the accuracy of the signature in predicting prognosis.

The GSE13507 dataset was used as the test cohort to verify the prognostic value of the novel signature, and it was also divided into two different subgroups using the same cutoff value as in the TCGA dataset. A survival discrepancy between the two subgroups was well exhibited using K–M curves ($P < 0.001$; Fig. 8G). ROC analysis also suggested that the novel signature could accurately predict the GSE13507 dataset (AUC values at 1 year, 3 years, and 5 years: 0.746, 0.680, and 0.653, respectively; Fig. 8H). Figure 8I also shows the good predictive power of the signature.

The novel signature can predict the response rates to immunotherapy

To further explore the potential value of the novel signature, we performed an analysis of the relationship between it and immunotherapy in BLCA patients. First, we found it has higher expression of immune checkpoint genes such as *CD274*, *CD276*, and *CTLA4* in high-risk group (Fig. 9A). The results of the seven-step cancer-immunity cycle analysis showed that the high-risk patients had higher activity in step 1 (release of cancer cell antigens), while they had lower activity in step 4 (trafficking of immune cells to tumors) and step 5 (infiltration of immune cells to tumors) (Fig. 9B). These results revealed that there may be an immune-inhibited TME in the high-risk group. Then, the different analyses of IPS revealed that the low-risk subgroup had a higher IPS score than the high-risk subgroup, which implied that the low-risk subgroup might have a better response rate to immunotherapy than the high-risk subgroup (all $P < 0.05$; Fig. 9C). Additionally, we used the "IMvigor 210" dataset to verify this claim, and the results showed that the high-risk subgroup had a poorer OS than the low-risk subgroup ($P < 0.001$; Fig. 9D) and that the low-risk subgroup had a better response rate to atezolizumab than the high-risk subgroup ($P = 0.03$; Fig. 9E).

The novel signature can predict drug sensitivity in bladder cancer

We conducted a drug sensitivity analysis of commonly used chemotherapeutics and targeted drugs for BLCA and found that the high-risk group had a lower IC₅₀ among common chemotherapeutics (including cisplatin (Fig. 10A), mitomycin-c (Fig. 10B), paclitaxel (Fig. 10C), and docetaxel (Fig. 10D)). However, it has a higher IC₅₀ in common targeted drugs (including erlotinib (Fig. 10E), lapatinib (Fig. 10F), nilotinib (Fig. 10G), and

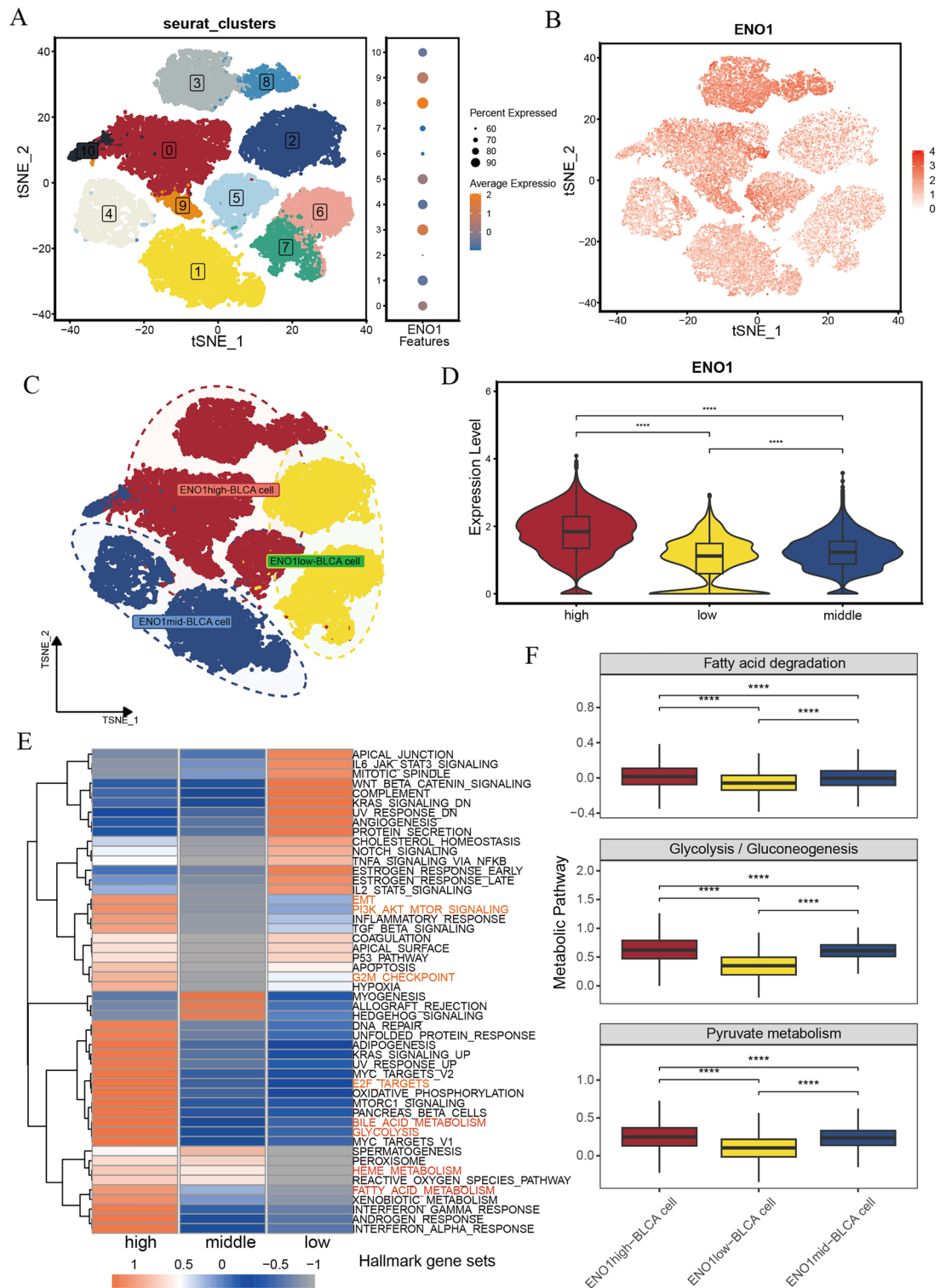


Figure 6. There was heterogeneity between ECs with different ENO1 expression levels. **(A)** Epithelial Cells were classified into 11 clusters with the t-SNE algorithm in GSE135337. **(B)** The tSNE map shows the expression levels in every cell. **(C)** Annotations for epithelial cell subtypes. **(D)** The differential expression of ENO1 in different subtypes of epithelial cells. **(E)** The heatmap shows the activities of hallmark pathways. **(F)** The differential activity of several metabolic pathways between different subtypes of epithelial cells. **** $P < 0.0001$; *** $0.001 < P < 0.01$; ** $0.01 < P < 0.05$; ns: $P > 0.05$.

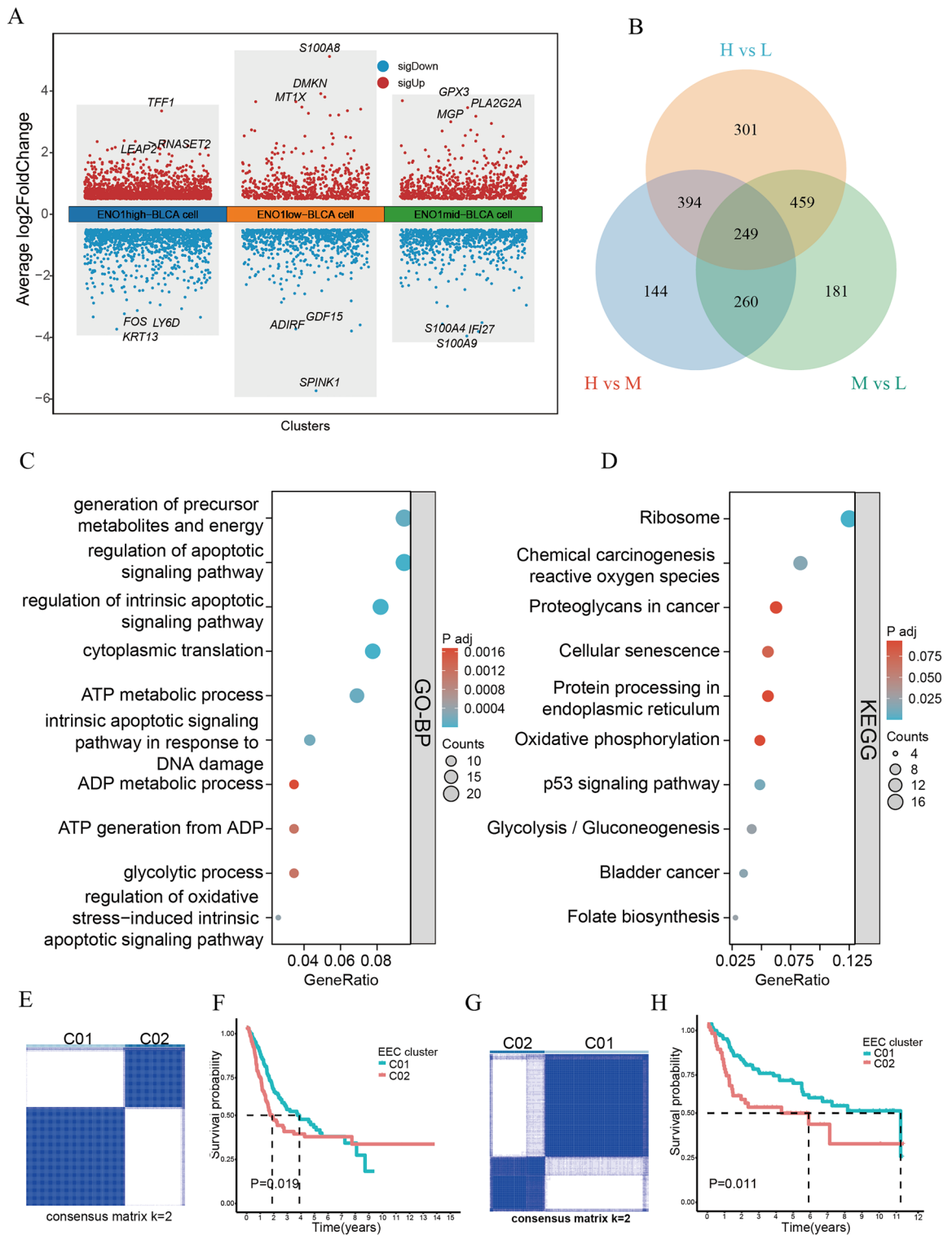


Figure 7. The function of hub genes and prognostic value. (A) The Manhattan map shows the differentially expressed genes. (B) Venn diagram showing the intersection between different differentially expressed genes. (C) The results of GO-BP analysis. (D) The results of KEGG analysis. (E) The consensus heatmap shows that the BLCA patients were divided into two distinct clusters when k = 2 in TCGA. (F) Kaplan–Meier survival curve of OS between different clusters in TCGA. (G) The consensus heatmap shows that the BLCA patients were divided into two distinct clusters when k = 2 in GSE13507. (H) Kaplan–Meier survival curve of OS between different clusters in GSE13507.

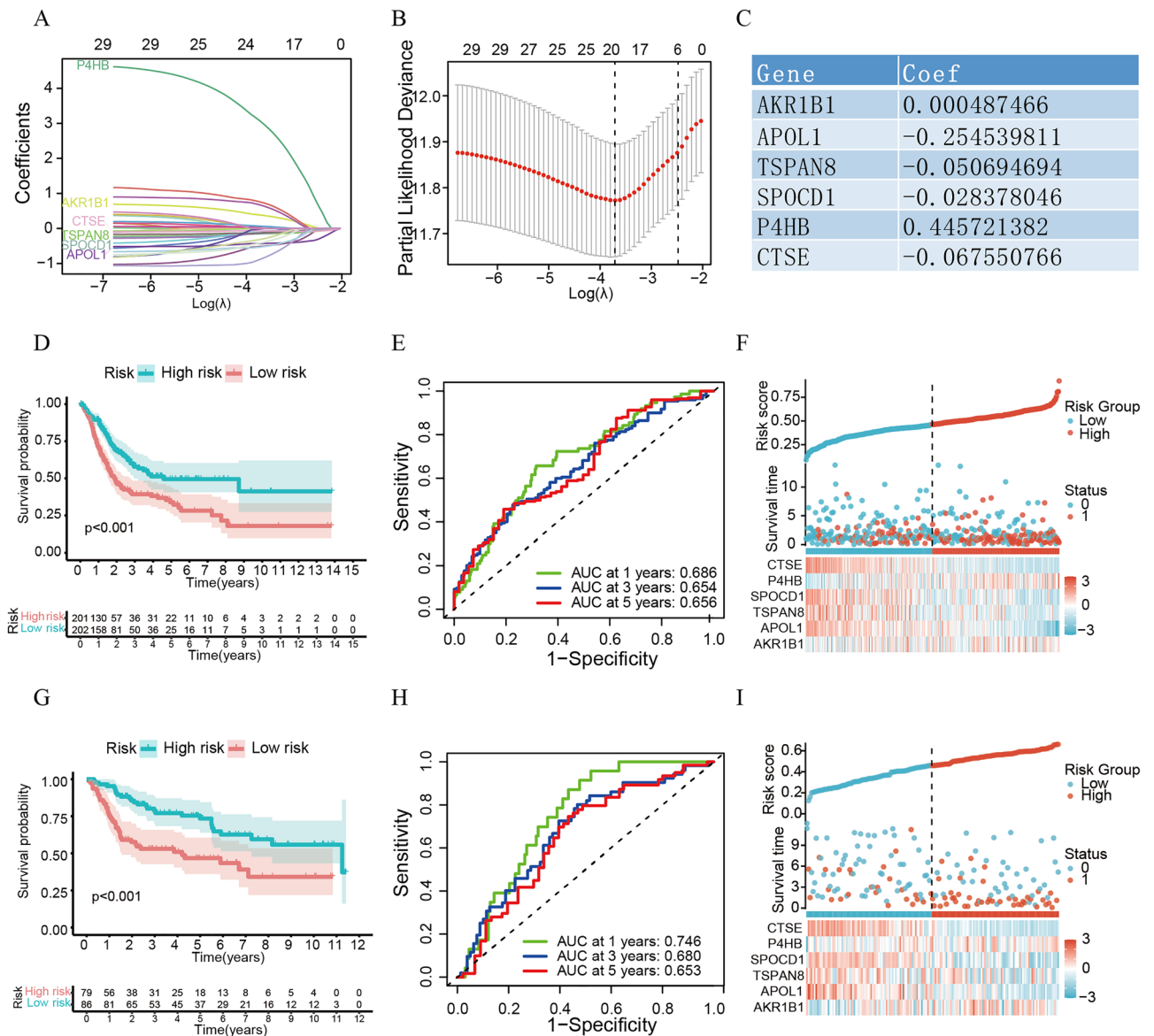


Figure 8. The novel signature can precisely predict the prognosis of BLCA patients. (A) LASSO coefficient profiles of the 29 hub genes. (B) Plots of the tenfold cross-validation error rates. (C) The coefficients of 6 candidate genes. (D) Kaplan–Meier survival curve of OS between the high- and low-risk groups in TCGA. (E) The ROC curve of the novel signature in TCGA. (F) Distribution of risk score, survival status and genes expressed in TCGA. (G) Kaplan–Meier survival curve of OS between the high- and low-risk groups in TCGA. (H) The ROC curve of the novel signature in TCGA. (I) Distribution of risk score, survival status and genes expressed in TCGA.

gefinitib (Fig. 10H)). These results suggested that high-risk patients may benefit more from chemotherapy and that low-risk patients may benefit more from targeted therapy.

Construction and evaluation of a prognostic nomogram

Supplementary Fig. 4A displays the results of univariate analysis. Age, N stage, and risk score were defined as independent prognostic factors in the TCGA dataset using multivariate Cox regression (all $P < 0.05$; Supplementary Fig. 4B). Then, we combined age, N stage and risk score to construct a prognostic nomogram (Fig. 11A). Calibration curves demonstrated an excellent fit regarding the predicted versus observed 1-, 3-, and 5-year OS of the BLCA patients (Fig. 11B). Moreover, the ROC curves exhibited better predictive capability in the current nomogram to assess the 1-, 3- and 5-year OS than risk score, age, N stage and risk scores published by Zhu et al., Chen et al., and Cao et al. (the values of the nomogram's AUCs at 1 year, 3 years, and 5 years were 0.762, 0.730, and 0.714, respectively; Fig. 11C–E). Additionally, DCA revealed the superiority of the current nomogram over risk score, age, and N stage in predicting 1-, 3-, and 5-year OS (Fig. 11F–H).

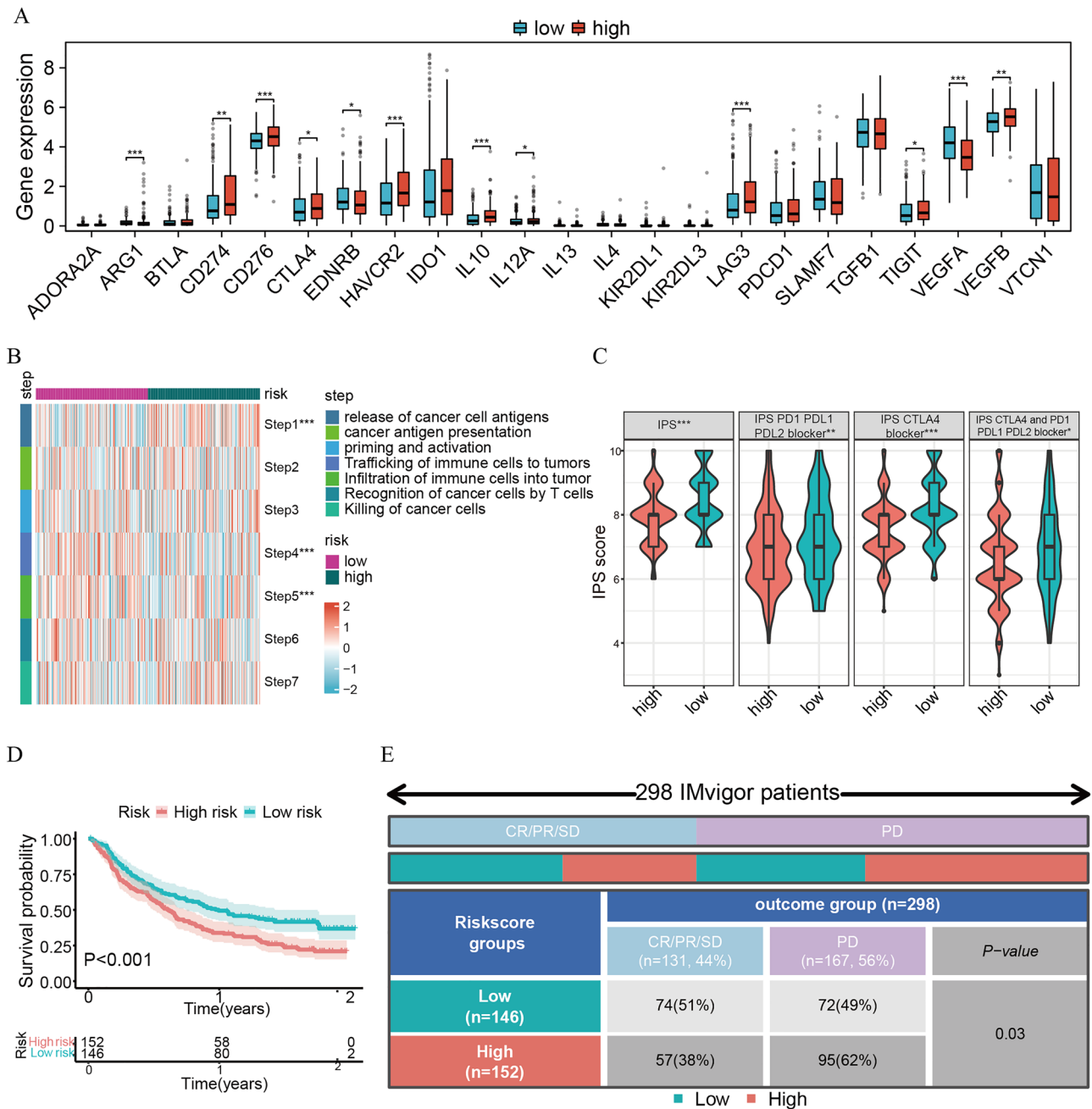


Figure 9. The novel signature can predict the response rates to immunotherapy. **(A)** The differential expression of immune checkpoint genes between high- and low-risk subgroups in TCGA. **(B)** The heatmap shows the differences in the seven steps of the cancer-immunity cycle analysis in TCGA. **(C)** The different IPS scores between high- and low-risk subgroups in TCGA. **(D)** Kaplan–Meier survival curve of OS between the high- and low-risk groups in the IMvigor 210 cohort. **(E)** Distribution of the immune response to immunotherapy therapy in different risk subgroups in the IMvigor 210 cohort.

Discussion

In this study, the prognostic role of *ENO1* in BLCA and its association with CD8+ T-cell exhaustion were analyzed by combining bulk RNA-seq and scRNA-seq data. In addition, we found heterogeneity among ECs with different *ENO1* expression levels and constructed a prognostic signature based on differentially expressed genes among ECs to predict prognosis and treatment responses.

First, through the TCGA-BLCA and GSE13507 data, we found that *ENO1* expression was upregulated in tumor tissue and positively associated with poor prognosis. The FPH cohort also confirmed this conclusion. In recent years, *ENO1* has been characterized by (1) cell surface localization; (2) high expression in cancer cells; and (3) its expression being positively associated with poor prognosis^{18,45}, which has been considered a novel tumor marker and therapeutic target, consistent with our conclusion. In addition, some studies have shown that

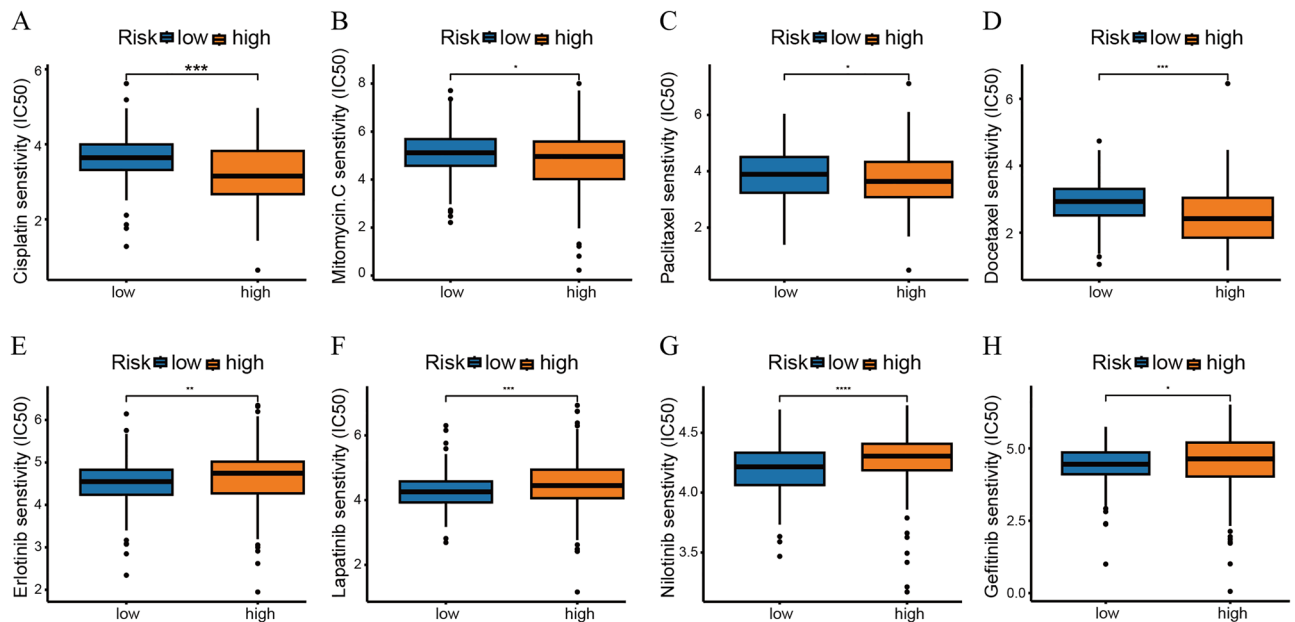


Figure 10. The novel signature can predict drug sensitivity. The different IC50 values of (A) cisplatin, (B) mitomycin-c, (C) paclitaxel, (D) docetaxel, (E) erlotinib, (F) lapatinib, (G) nilotinib, and (H) gefitinib.

silencing *ENO1* expression can inhibit cancer invasion⁴⁶, migration and metastasis⁴⁷, which was also confirmed in vitro in our study.

Recent studies have found that T-cell dysfunction is associated with glucose metabolism disorders⁴⁸, and the competition between tumor cells and CD8+ T cells for limited glucose leads to reduced CD8+ T-cell effector function⁴⁹. However, Chang et al. found that in exhausted CD8+ T cells in vitro, it was difficult to increase their effector capacity even if superphysiological levels of glucose were given⁵⁰. Interestingly, by single-cell sequencing data analysis of CD8+ T cells, we found that *ENO1* and inhibitory receptors such as *LAG3* were upregulated with the progression of CD8+ T-cell exhaustion in our study, which was consistent with the results of L.F. Gemta's study and suggested that *ENO1* may undergo posttranslational modification in exhausted CD8+ T cells^{17,51}.

ENO1 can, through the regulation of the cell cycle⁵² and apoptosis, maintain cancer cell proliferation and resistance to cell death⁵³, and through the induction of EMT, promote invasion and metastasis⁵⁴. In the current study, we found significant heterogeneity between epithelial cells with different *ENO1* expression levels. *ENO1*^{high}-BLCA cells promote BLCA progression mainly by affecting metabolism, the cell cycle and EMT. Then, the hub genes were defined as the intersection of differentially expressed genes between different ECs. Functional enrichment analysis showed that the hub genes were enriched in energy metabolism, apoptosis regulation, and multiple oncogenic pathways.

LASSO can effectively screen unimportant variables and prevent overfitting. Therefore, we chose LASSO to construct a prognostic signature. We used TCGA as the training set and GSE13507 as the validation set to construct a novel signature consisting of 6 genes by LASSO regression analysis. Then, BLCA patients were divided into high-risk group and low-risk group according to the risk score of each sample. The results showed that the risk score could successfully predict the OS of BLCA patients, and the OS of high-risk group was significantly worse than that of low-risk group. The ROC curve also indicated that the novel signatures had good prognostic ability. These results suggested that the *ENO1*-associated epithelial prognostic signature played a carcinogenic role in BLCA progression, which was consistent with the function of *ENO1*.

Considering the high tumor mutation burden of BLCA, immune checkpoint inhibitors (ICIs) have been an alternative treatment with promising results. However, the clinical efficacy of ICI therapy for BLCA patients is far from satisfactory, with a response rate to ICIs as low as 20–30%^{55–57}. The lack of precise biomarkers to predict the response to ICIs might be quite a reason; therefore, it is urgently needed to identify reliable prognostic biomarkers to increase the proportion of responders to ICIs in BLCA. In this study, the novel signature was also found to be correlated with IPS. This result indicated that the current signature might be taken as an alternative signature to predict the response to ICIs, which was confirmed by the IMvigor 210 cohort, which consisted of 298 urothelial carcinoma patients receiving atezolizumab (a PD-L1 inhibitor). However, these findings need further validation.

There were several shortcomings in our study. First, considering that consensus was not reached on CD8+ T-cell exhaustion genes, we selected exhaustion genes from the published records, which would result in selection bias and publication bias. Second, the novel signature exhibited good prediction of prognosis and treatment response, but it would be better if it was verified by the cohort from our center. Third, single-cell analysis revealed the relationship between *ENO1* and CD8+ T-cell exhaustion using a public dataset, and we will continue to work on these in vitro and in vivo studies.

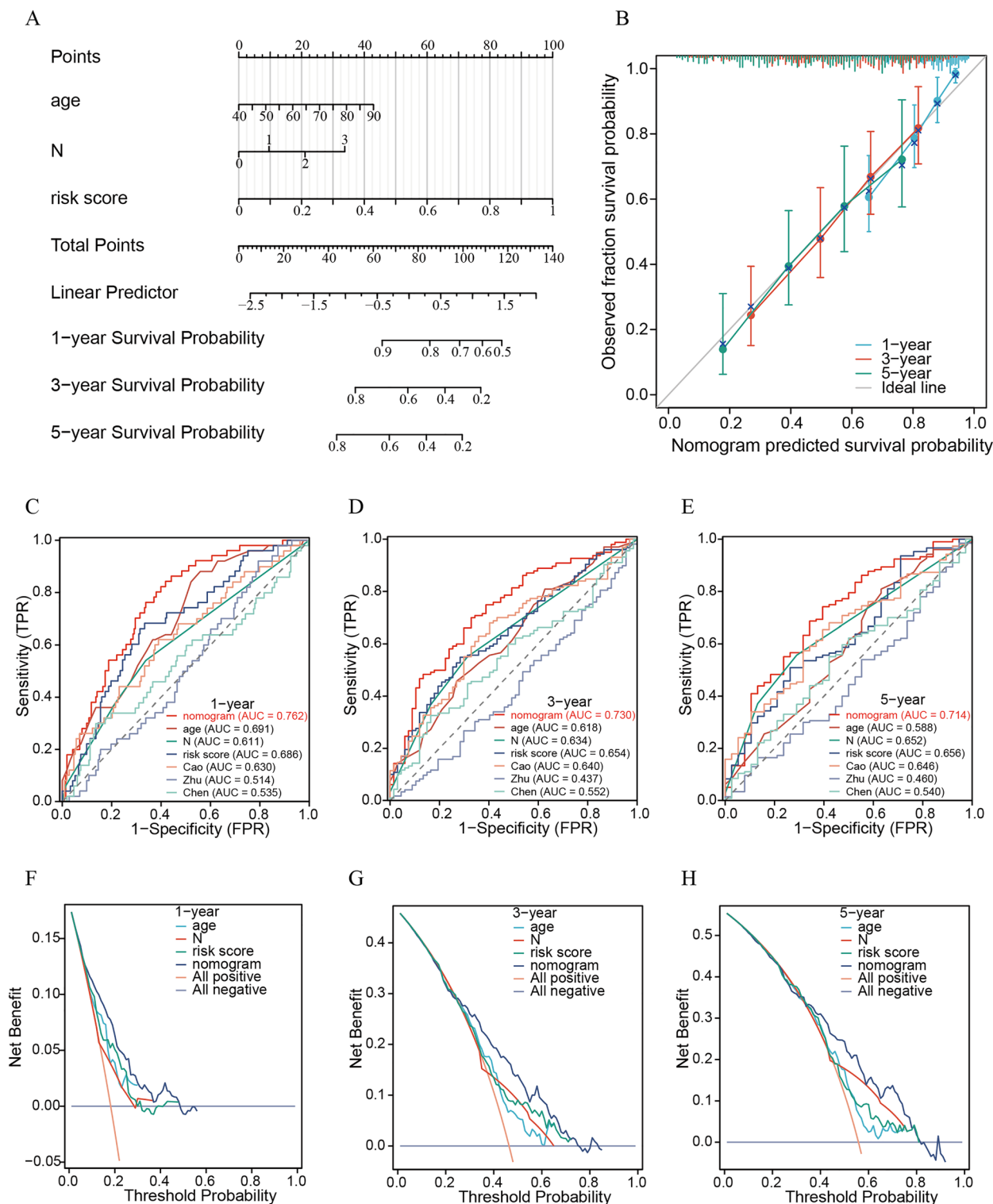


Figure 11. The nomogram was more precise in predicting the prognosis of BLCA patients than other signatures. **(A)** The prognostic nomogram constructed based on the risk score and clinicopathological parameters predicted the survival rate of TCGA-BLCA patients at 1, 3, and 5 years. **(B)** Calibration curves showing the concordance between predicted and observed 1-, 3-, and 5-year survival rates. AUCs of the nomogram, risk score and other signatures in ROC analysis were calculated at **(C)** 1-, **(D)** 3-, and **(E)** 5-year OS times in the TCGA-BLCA cohort. Decision curve analyses (DCA) for the nomogram, EETS and other signatures at **(F)** 1-, **(G)** 3-, and **(H)** 5 years to assess clinical utility in the TCGA-BLCA cohort.

Conclusion

In conclusion, by integrating the results of bulk RNA-seq, protein, and scRNA-seq, our work revealed that *ENO1* was a prognostic marker and might participate in CD8+ T-cell exhaustion within BLCA. Then, there was heterogeneity between ECs with different *ENO1* expression levels, and based on these differentially expressed genes, we constructed a novel signature with good prediction of prognosis and treatment response among BLCA patients.

Data availability

Publicly available datasets were analyzed in this study. These data can be found here: TCGA (<http://portal.gdc.cancer.gov/>) and GEO (www.ncbi.nlm.nih.gov/) under the accession numbers GSE13507, GSE135337 and GSE149652. The RNA-seq profiles and clinical data of the “IMvigor 210” cohort were derived from <http://research-pub.gene.com/IMvigor210CoreBiologies/>.

Received: 18 September 2023; Accepted: 20 January 2024

Published online: 25 January 2024

References

- Patel, V. G., Oh, W. K. & Galsky, M. D. Treatment of muscle-invasive and advanced bladder cancer in 2020. *CA Cancer J. Clin.* **70**(5), 404–423 (2020).
- Saginala, K. *et al.* Epidemiology of bladder cancer. *Med. Sci. (Basel)* **8**(1), 15 (2020).
- Sung, H. *et al.* Global cancer statistics 2020: GLOBOCAN estimates of incidence and mortality worldwide for 36 cancers in 185 countries. *CA Cancer J. Clin.* **71**(3), 209–249 (2021).
- Cumberbatch, M. G. K. *et al.* Epidemiology of bladder cancer: A systematic review and contemporary update of risk factors in 2018. *Eur. Urol.* **74**(6), 784–795 (2018).
- Mari, A. *et al.* Genetic determinants for chemo- and radiotherapy resistance in bladder cancer. *Transl. Androl. Urol.* **6**(6), 1081–1089 (2017).
- Fu, H. *et al.* Identification and validation of stromal immunotype predict survival and benefit from adjuvant chemotherapy in patients with muscle-invasive bladder cancer. *Clin. Cancer Res.* **24**(13), 3069–3078 (2018).
- Zhou, L. *et al.* Tumor-infiltrating neutrophils predict benefit from adjuvant chemotherapy in patients with muscle invasive bladder cancer. *Oncoimmunology* **6**(4), e1293211 (2017).
- Fu, Q. F. *et al.* Alpha-enolase promotes cell glycolysis, growth, migration, and invasion in non-small cell lung cancer through FAK-mediated PI3K/AKT pathway. *J. Hematol. Oncol.* **8**, 22 (2015).
- Zhang, L., Wang, H. & Dong, X. Diagnostic value of α -enolase expression and serum α -enolase autoantibody levels in lung cancer. *J. Bras. Pneumol.* **44**(1), 18–23 (2018).
- Zhang, J. *et al.* Silencing of ENO1 inhibits the proliferation, migration and invasion of human breast cancer cells. *J. BUON* **25**(2), 696–701 (2020).
- Qiao, H. *et al.* Enolase1 overexpression regulates the growth of gastric cancer cells and predicts poor survival. *J. Cell. Biochem.* **120**(11), 18714–18723 (2019).
- Zhan, P. *et al.* α -enolase promotes tumorigenesis and metastasis via regulating AMPK/mTOR pathway in colorectal cancer. *Mol. Carcinogen.* **56**(5), 1427–1437 (2017).
- Principe, M. *et al.* Alpha-enolase (ENO1) controls α v/ β 3 integrin expression and regulates pancreatic cancer adhesion, invasion, and metastasis. *J. Hematol. Oncol.* **10**(1), 16 (2017).
- Viallard, C. & Larrivée, B. Tumor angiogenesis and vascular normalization: Alternative therapeutic targets. *Angiogenesis* **20**(4), 409–426 (2017).
- Capello, M. *et al.* Targeting the Warburg effect in cancer cells through ENO1 knockdown rescues oxidative phosphorylation and induces growth arrest. *Oncotarget* **7**(5), 5598–5612 (2016).
- La-Rocca, C. *et al.* Immunometabolic profiling of T cells from patients with relapsing-remitting multiple sclerosis reveals an impairment in glycolysis and mitochondrial respiration. *Metabol. Clin. Exp.* **77**, 39–46 (2017).
- Gemta, L. F. *et al.* Impaired enolase 1 glycolytic activity restrains effector functions of tumor-infiltrating CD8(+) T cells. *Sci. Immunol.* **4**(31), 145 (2019).
- Huang, C. K. *et al.* ENO1 and cancer. *Mol. Ther. Oncolyt.* **24**, 288–298 (2022).
- Song, Y. *et al.* Alpha-enolase as a potential cancer prognostic marker promotes cell growth, migration, and invasion in glioma. *Mol. Cancer* **13**(1), 65 (2014).
- Potter, S. S. Single-cell RNA sequencing for the study of development, physiology and disease. *Nat. Rev. Nephrol.* **14**(8), 479–492 (2018).
- Necchi, A. *et al.* Atezolizumab in platinum-treated locally advanced or metastatic urothelial carcinoma: Post-progression outcomes from the phase II IMvigor210 study. *Ann. Oncol.* **28**(12), 3044–3050 (2017).
- Oh, D. Y. *et al.* Intratumoral CD4(+) T cells mediate anti-tumor cytotoxicity in human bladder cancer. *Cell* **181**(7), 1612–25.e13 (2020).
- Lai, H. *et al.* Single-cell RNA sequencing reveals the epithelial cell heterogeneity and invasive subpopulation in human bladder cancer. *Int. J. Cancer* **149**(12), 2099–2115 (2021).
- Mangiola, S., Doyle, M. A. & Papenfuss, A. T. Interfacing Seurat with the R tidy universe. *Bioinformatics* **37**(22), 4100–4107 (2021).
- Song, P. *et al.* Identification and validation of a novel signature based on NK Cell marker genes to predict prognosis and immunotherapy response in lung adenocarcinoma by integrated analysis of single-cell and bulk RNA-sequencing. *Front. Immunol.* **2022**, 13 (2022).
- Zhang, X. *et al.* Cell Marker: A manually curated resource of cell markers in human and mouse. *Nucl. Acids Res.* **47**(D1), D721–D728 (2018).
- Huang, Q. *et al.* Evaluation of cell type annotation R packages on single-cell RNA-seq data. *Genom. Proteom. Bioinform.* **19**(2), 267–281 (2021).
- Qiu, X. *et al.* Reversed graph embedding resolves complex single-cell trajectories. *Nat. Methods* **14**(10), 979–982 (2017).
- Wu, Y. *et al.* Spatiotemporal immune landscape of colorectal cancer liver metastasis at single-cell level. *Cancer Discov.* **12**(1), 134–153 (2022).
- Borowczak, J. *et al.* The prognostic role of CDK9 in bladder cancer. *Cancers (Basel)* **14**(6), 145 (2022).
- Huang, Z. *et al.* CBX7 suppresses urinary bladder cancer progression via modulating AKR1B10-ERK signaling. *Cell Death Dis.* **12**(6), 537 (2021).
- Hänzelmann, S., Castelo, R. & Guinney, J. GSEA: Gene set variation analysis for microarray and RNA-seq data. *BMC Bioinform.* **14**, 7 (2013).

33. Li, T. *et al.* TIMER: A web server for comprehensive analysis of tumor-infiltrating immune cells. *Cancer Res.* **77**(21), e108–e110 (2017).
34. Xu, L. *et al.* TIP: A web server for resolving tumor immunophenotype profiling. *Cancer Res.* **78**(23), 6575–6580 (2018).
35. Prior, F. W. *et al.* TCIA: An information resource to enable open science. *Annu. Int. Conf. IEEE Eng. Med. Biol. Soc.* **2013**, 1282–1285 (2013).
36. Kanehisa, M. & Goto, S. KEGG: Kyoto encyclopedia of genes and genomes. *Nucl. Acids Res.* **28**(1), 27–30 (2000).
37. Kanehisa, M. Toward understanding the origin and evolution of cellular organisms. *Protein Sci.* **28**(11), 1947–1951 (2019).
38. Kanehisa, M. *et al.* KEGG for taxonomy-based analysis of pathways and genomes. *Nucl. Acids Res.* **51**(D1), D587–D592 (2023).
39. Yu, G. *et al.* clusterProfiler: An R package for comparing biological themes among gene clusters. *Omics* **16**(5), 284–287 (2012).
40. Wilkerson, M. D. & Hayes, D. N. ConsensusClusterPlus: A class discovery tool with confidence assessments and item tracking. *Bioinformatics* **26**(12), 1572–1573 (2010).
41. Kang, J. *et al.* LASSO-based machine learning algorithm for prediction of lymph node metastasis in T1 colorectal cancer. *Cancer Res. Treat.* **53**(3), 773–783 (2021).
42. Engebretsen, S. & Bohlin, J. Statistical predictions with glmnet. *Clin. Epigenet.* **11**(1), 123 (2019).
43. Geeleher, P., Cox, N. & Huang, R. S. pRRophetic: An R package for prediction of clinical chemotherapeutic response from tumor gene expression levels. *PLoS One* **9**(9), e107468 (2014).
44. Kurachi, M. CD8(+) T cell exhaustion. *Semin. Immunopathol.* **41**(3), 327–337 (2019).
45. Qiao, G. *et al.* Enolase 1, a moonlighting protein, as a potential target for cancer treatment. *Int. J. Biol. Sci.* **17**(14), 3981–3992 (2021).
46. Hsiao, K. C. *et al.* Surface α -enolase promotes extracellular matrix degradation and tumor metastasis and represents a new therapeutic target. *PLoS One* **8**(7), e69354 (2013).
47. Kumari, S. & Malla, R. New insight on the role of plasminogen receptor in cancer progression. *Cancer Growth Metastasis* **8**, 35–42 (2015).
48. Chan, Y. T. *et al.* Immune checkpoint molecules and glucose metabolism in HIV-Induced T cell exhaustion. *Biomedicines* **10**(11), 2809 (2022).
49. Ho, P. C. *et al.* Phosphoenolpyruvate is a metabolic checkpoint of anti-tumor T cell responses. *Cell* **162**(6), 1217–1228 (2015).
50. Chang, C. H. *et al.* Metabolic competition in the tumor microenvironment is a driver of cancer progression. *Cell* **162**(6), 1229–1241 (2015).
51. Zhou, W. *et al.* Mass spectrometry analysis of the post-translational modifications of alpha-enolase from pancreatic ductal adenocarcinoma cells. *J. Proteom. Res.* **9**(6), 2929–2936 (2010).
52. Zhang, Z. *et al.* CCDC65, a gene knockout that leads to early death of mice, acts as a potentially novel tumor suppressor in lung adenocarcinoma. *Int. J. Biol. Sci.* **18**(10), 4171–4186 (2022).
53. Zhang, T. *et al.* ENO1 suppresses cancer cell ferroptosis by degrading the mRNA of iron regulatory protein 1. *Nat. Cancer* **3**(1), 75–89 (2022).
54. Gu, J. *et al.* ENO1 contributes to 5-fluorouracil resistance in colorectal cancer cells via EMT pathway. *Front. Oncol.* **12**, 1013035 (2022).
55. Cancer Genome Atlas Research Network. Comprehensive molecular characterization of urothelial bladder carcinoma. *Nature* **507**(7492), 315–322 (2014).
56. Rhea, L. P. *et al.* Role of immunotherapy in bladder cancer. *Cancer Treat. Res. Commun.* **26**, 100296 (2021).
57. Pettenati, C. & Ingersoll, M. A. Mechanisms of BCG immunotherapy and its outlook for bladder cancer. *Nat. Rev. Urol.* **15**(10), 615–625 (2018).

Acknowledgements

We sincerely thank the researchers and study participants for their contributions to this study. We are also grateful to the data providers of the various public databases.

Author contributions

Z.S.: Conceptualization, Methodology, Data curation, Validation, Writing - original draft, Writing - review & editing. L.Y.: Writing - review & editing. Y.H.: Investigation, Methodology, Data curation, Validation. J.C.: Writing - review & editing. G.Z.: Writing - review & editing. Z.L.: Conceptualization, Methodology, Supervision, Data curation, Validation, Writing - review & editing.

Funding

Fujian Provincial Health Technology Project (No.2016-CX-4). Fujian Provincial Finance Project (No.(2021)848).

Competing interests

The authors declare no competing interests.

Additional information

Supplementary Information The online version contains supplementary material available at <https://doi.org/10.1038/s41598-024-52573-8>.

Correspondence and requests for materials should be addressed to J.C., G.Z. or Z.L.

Reprints and permissions information is available at www.nature.com/reprints.

Publisher's note Springer Nature remains neutral with regard to jurisdictional claims in published maps and institutional affiliations.



Open Access This article is licensed under a Creative Commons Attribution 4.0 International License, which permits use, sharing, adaptation, distribution and reproduction in any medium or format, as long as you give appropriate credit to the original author(s) and the source, provide a link to the Creative Commons licence, and indicate if changes were made. The images or other third party material in this article are included in the article's Creative Commons licence, unless indicated otherwise in a credit line to the material. If material is not included in the article's Creative Commons licence and your intended use is not permitted by statutory regulation or exceeds the permitted use, you will need to obtain permission directly from the copyright holder. To view a copy of this licence, visit <http://creativecommons.org/licenses/by/4.0/>.

© The Author(s) 2024